Decomposing photoplethysmogram waveforms into systolic and diastolic waves, with application to hyperbaric environments

Alberto Hernando, María Dolores Peláez-Coca, Eduardo Gil.

Abstract*—*Objective: **A new algorithm to decompose the photoplethysmogram (PPG) pulse in two waves related with the systolic and diastolic parts, was applied to identify alterations in the morphology of the PPG pulse due to the pressure.** ***Approach:*** **Each pulse was decomposed into two waves: the first one a Gaussian related with the systolic peak, and the second one was modelled as a lognormal curve associated with the diastolic part. From these two waves, 13 parameters related with the width (W1, W2 and W2/W1), the time instant (T1, T2, T21, T_{BB}), the amplitude (A1, A2, A2/A1) and the areas (D1, D2, D2/D1) were estimated. These parameters were computed from subjects inside a hyperbaric chamber, involving five stages at different pressure: 1 atm, 3 atm, 5 atm, 3 atm and 1 atm.** ***Main results:*** **There was a significant increase in the values of A1, A2, W1, T1, and D1, and a decrease in the ratios when the pressure increased, that suggest a vasoconstriction when the pressure increased. There is also an increase in the values of T_{BB}, T2, T12, and W2 along the protocol, that implies a dependency of some parameters with the pulse-to-pulse interval.** ***Significance:*** **This methodology allows extracting a large set of parameters related with the PPG morphology that are affected by the change of pressure inside hyperbaric environments.**

***Index Terms*—PPG morphology, pulse decomposition analysis, hyperbaric environments, lognormal.**

I. Introduction

Photoplethysmography (PPG) is an optical measurement technique that can be used to detect blood volume changes in the microvascular bed of tissues [17]. PPG morphology can provide information about vascular assessment or arterial compliance, since pulse pressure propagation in arteries causes alterations in blood volume and therefore changes in the PPG pulse shape [18], [19]. In the bibliography, there are several studies that give some physiological interpretation to the variation of pulse waveform parameters. In [20], variations in PPG amplitude is directly proportional to vascular distensibility; in [21], a reduction in the pulse amplitude may be directly attributable to a loss of central arterial pressure, which could be related to an activation of the sympathetic system of the subject; in at least two studies [23], [24], the reflection index (RI), which is the ratio between the amplitude of the systolic and the diastolic peaks of the PPG, could be used as an estimator of the vascular resistance of the peripheral arteries; also the ratio of two PPG subareas (divided at the dicrotic notch) could be an indicator of total peripheral resistance [26]; even some studies suggest that PPG width is correlated with the systemic vascular resistance [27]. Also, there are some studies that analyze the variations of some pulse morphological parameters during different stages, finding differences among basal and low stress states [28] among different types of exercise [29], [30] or among different postural changes [31]. Therefore, in this work, PPG morphological parameters are extracted in different atmospheric pressure stages, to see if they differ or not due to the pressure.

The parameters mentioned above are extracted from the original PPG waveform or from its first or second derivatives. In other works, those parameters can be extracted from PPG pulses modelled by a linear combination of several waves. This methodology is called Pulse Decomposition Analysis (PDA). The premise of the PDA model is that the peripheral arterial pressure pulse is a superposition of individual component pressure pulses, the first of which is due to the left ventricular ejection from the heart while the remaining component pressure pulses are reflections and re-reflections [32]. Most of the PDA techniques try to fit a model based on a superposition of waves at once, based on different shapes including Gaussians [32], [33], [34], lognormals [35], Rayleighs [36] or a combination of them [37], [38]. However, not always the decomposed waves match with the systolic and diastolic peaks, or they do not have enough amplitude to extract some parameters as the reflection index. Another type of approach is to extract the waves one-by-one, as in [40], [41] instead of fitting a several-waves-model at once. In these two works, the authors proposed the use of three Gaussians waves to decompose the entire pulse, which usually get worse fitting at the end of the pulse due to the asymmetry between the up-slope and the down-slope of the PPG pulse.

Therefore, in this work, we proposed a new technique to estimate parameters from the pulse waveform. A first wave related to the systole is extracted directly from the PPG pulse concatenating the up-slope (from the beginning till the absolute maximum) with itself horizontally flipped. Then a second wave related with the diastole is modelled by a lognormal wave. From these two waves, the amplitude, the time instant, the width, the area and some ratios are extracted. This algorithm is applied into the hyperbaric chamber dataset to identify alterations in the morphology of the PPG pulse due

A. Hernando is with Ioon Technologies, Madrid, Spain.

M.D. Peláez-Coca is with Centro Universitario de Defensa (CUD), Academia General Militar (AGM), Zaragoza, Spain.

E. Gil is with Centro de Investigación Biomédica en Red Bioingeniería, Biomateriales y Nanomedicina (CIBER-BBN), Madrid, Spain.

M.D. Peláez-Coca and E. Gil are with BSICoS Group, Aragón Institute of Engineering Research (I3A), IIS Aragón, University of Zaragoza, Zaragoza, Spain.

to the exposure of the subjects to pressure changes.

II. Materials

A total of 23 subjects (22 males and 1 female), with a mean age of 27.74 5.15 years, with a mean height of 176.45 5.73 meters and a mean weight of 78.18 8.63 kilograms, were recorded inside the hyperbaric chamber of the Hospital General de la Defensa de Zaragoza, with the approval from the "Comité de ética de la investigación con medicamentos de la inspección general de sanidad de la Defensa" ethics committee. It must be highlighted that 20 subjects out of 23, the 86.96% of the total study population, were military personnel.

The protocol consisted in five different stages involving 5 minutes (min) stops at different atmospheres (atm): 1 atm (sea level), 3 atm (simulating 20 meters depth) and 5 atm (simulating 40 meters depth), and subsequently returning to 3 atm and 1 atm. The protocol inside the chamber had a duration of about two hours and most of the time was spent in the decompression stops between 3 atm and 1 atm, as recommended in standard decompression tables. In 19 subjects, this decompression time was 44 min, distributed as follows: 2 min at 1.9 atm, 16 min at 1.6 atm and 26 min at 1.3 atm. In the rest of the cases, this time was slightly fewer, but always upper than 30 min. A schematic representation of this protocol is shown in Table I.

During the entire test, subjects remained relaxed and sitting comfortably, and the chamber was correctly ventilated to avoid major changes in temperature and humidity. Subjects remained in silence and without perform movements during basal stages. Therefore, a total of five stages, referred to as S1D, S3D, S5, S3A and S1A (S from stage; the number reflects the pressure, in atm; the letter D or A refers to descent or ascent) were studied.

Recordings were performed using a Nautilus device [42], which allows recording the PPG signal on the middle finger of the non-dominant hand with a sampling frequency (fs) of 1000 Hz and the atmospheric pressure (fs = 250 Hz) inside the chamber.

III. Methods

A. PPG preprocessing

A low-pass finite-impulse-response filter with a cut-off frequency of 10 Hz was applied to the PPG to attenuate noise [43]. Artefactual pulses were suppressed by using the artefact detector described in [44]. Later, the PPG pulses were automatically detected and the basal points (n_{Bi}) of each pulse were obtained using an algorithm based on a low-pass differentiator filter [45]. All these filters are forward-backward filters, that maintain the morphology of the pulse wave. Then, the baseline of the PPG signal was estimated by cubic-spline-interpolation of n_{Bi} and subsequently subtracted to ensure that each PPG pulse begins and ends with zero amplitude. Finally, for each subject, all the PPG pulses were normalized with respect to the pulse with the highest amplitude in the five stages according to the protocol (see Table I), to ensure that the maximum amplitude is one. The resulting PPG signal was called $x_{PPG}(n)$.

B. Pulse decomposition analysis

Once each pulse was isolated, two main waves were extracted, the first one reflecting the systole and the second one related with the diastole, trying to match the maximum of each wave with the two peaks. All the entire process that reflects the pulse decomposition analysis is illustrated in Fig. 1. Next, an explanation of each phase of this process is given, and a reference to this Figure will be done to clarify the entire process and help the reader's understanding.

To extract the first wave related to the systole part of each pulse (*i-th*), the algorithm explained in [40] was applied as follows:

1) Set the beginning of the up-slope wave as the previous to the first non-zero-amplitude sample (in this case, n_{Bi}).
2) Set the end of the up-slope wave as the time instant of the absolute maximum (n_{Ai}).
3) Estimate the systolic wave ($y_{S,i}(n)$) by concatenating the up-slope with itself horizontally flipped, as it is shown in Eq. 1, assuming that it is symmetric.

$$y_{S,i}(n) = \begin{cases} x_{PPG}(n), & n \in [n_{Bi}, n_{Ai}] \\ x_{PPG}(-n + 2n_{Ai}), & t \in [n_{Ai}, 2n_{Ai} - n_{Bi}] \\ 0, & otherwise \end{cases} \quad (1)$$

Therefore, this first wave represents the part of the PPG associated with the systolic peak (see parts a, b, and c of Fig.1).

Then, this wave was subtracted from the original PPG waveform to characterize the diastolic part, obtaining the residual pulse waveform ($r^1_{PPG}(n)$, see part d of Fig.1). Then, the location of the maximum of this new wave is found, and depending on its location, two possible alternatives can be followed:

- On the one hand, if the temporal location of the maximum of $r^1_{PPG}(n)$ is higher than the 35% of the pulse wave duration, this peak belongs to the diastolic part.
- On the other hand, if the temporal location of the maximum of $r^1_{PPG}(n)$ is lower, this implies that this maximum does not belong to the diastolic peak. Therefore, the same processing step explained for the first wave is repeated one more time, obtaining a transition wave ($y_{T,i}(n)$, see part e of Fig.1) that it is not used for extracting physiological parameters, but it is subtracted from the PPG pulse, obtaining another residual pulse waveform ($r^2_{PPG}(n)$), whose maximum is now related with the diastolic peak.

This temporal threshold of 35% has been determined experimentally, based on the assumption that left ventricular ejection time related with the systole usually lasts less than 35% of the pulse wave duration [46].

Finally, when the residual waveform related to the diastolic part was found ($r^1_{PPG}(n)$ or $r^2_{PPG}(n)$, see part f of Fig.1), it was modelled as a lognormal wave (as can be seen in Eq. 2) to be able to extract some characteristics as the amplitude, the width and the area under the curve. To do this modelling, first the residual waveform was normalized to the unit in amplitude and to 1000 samples in time by spline interpolation. Once

TABLE I
EXPLANATION OF THE PROTOCOL USED, SHOWING THE ATMOSPHERIC PRESSURE, THE DIFFERENT PARTS AND THEIR RESPECTIVE DURATIONS.

Pressure	1 atm (sea level)	1-3 atm	3 atm	3-5 atm	5 atm	5-3 atm	3 atm	3-1 atm	1 atm (sea level)
Explanation	S1D	Descending	S3D	Descending	S5	Ascending	S3A	Ascending	S1A
Duration	5 min	6-8 min	5 min	6-8 min	5 min	6-8 min	5 min	50-55 min	5 min

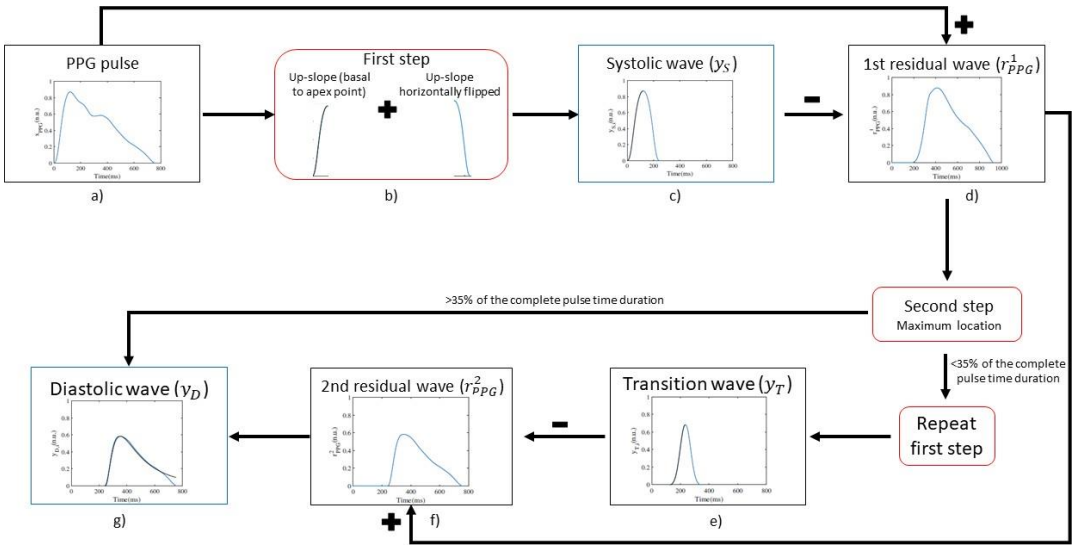

Fig. 1. Description of the pulse decomposition analysis algorithm, with the different steps remarked in red, the systolic and diastolic waves in blue and the resultant waves in black. From the original PPG pulse ($x_{PPG}(n)$, subfigure a), the wave related to the systolic peak ($y_{S,i}(n)$, subfigure c) is extracted by finding the up-slope and concatenating this part with itself horizontally flipped (first step, represented in subfigure b). Then, the first residual pulse waveform ($r^1_{PPG}(n)$, subfigure d) is obtained as the subtraction of $y_{S,i}(n)$ from $x_{PPG}(n)$. Later, if the time duration of the maximum of $r^1_{PPG}(n)$ is shorter than the 35% of the complete pulse time duration, a new wave ($y_{T,i}(n)$, subfigure e) not related with the diastolic peak is extracted, repeating the process described in the first step. In a similar way, the second residual pulse waveform ($r^2_{PPG}(n)$, subfigure f) is obtained as the subtraction of $y_{T,i}(n)$ from $r^1_{PPG}(n)$ and this wave is related with the diastolic peak and modelled as a lognormal wave ($y_{D,i}(n)$, subfigure g). If the time duration of the maximum of $r^1_{PPG}(n)$ is longer than the 35% of the complete pulse time duration, it is this wave to be modelled as a lognormal wave.

normalized, a lognormal wave was created with its values of μ and σ varying μ from μ_0-100 to μ_0+300 in steps of 25 (where μ_0 is the time location of the maximum) and σ from 0.2 to 1 in steps of 0.1 respectively. The values of μ and σ that minimize the mean-squared error between the lognormal wave and the residual pulse waveform were selected and the lognormal wave obtained was now reconverted to the original values of amplitude and time ($y_{D,i}(n)$, see part g of Fig.1).

$$f(x) = \frac{1}{\sqrt{2\pi\sigma}} \cdot e^{\frac{-(u-\mu)^2}{2\sigma^2}} \quad (2)$$

Finally, in Fig. 2, there is an example of the PPG pulse decomposition with three waves and with only two waves.

C. Pulse waveform characteristics

From the first wave associated with the systolic peak ($y_{S,i}(n)$) and from the lognormal associated with the diastolic peak ($y_{D,i}(n)$), several morphological features were extracted. The amplitude (A1 and A2) and the position of the maximum (T1 and T2) of the two waves were defined. The width (W1 and W2) was estimated as the full-width at half maximum since the end of the lognormal down-slope did not finish in the zero value. Also, the area under the curve from the top until the half maximum (D1 and D2) was computed. An example of these parameters can be seen in Fig. 3. The time delay between both waves (T12 = T2-T1), the reflection index (RI = A2/A1), the ratio between the widths (W2/W1), the ratio between the areas (D2/D1), and the pulse-to-pulse interval (T_{BB}), measured as the difference between consecutive n_{Bi}, were also calculated. These parameters were extracted from the five stages of the hyperbaric chamber dataset to see differences between the stages.

D. Statistical analysis

To minimize the effects of the inter-subject variability, the Relative Change (RC) of each parameter (Y) with respect to the reference stage (S1D), was calculated as a percentage:

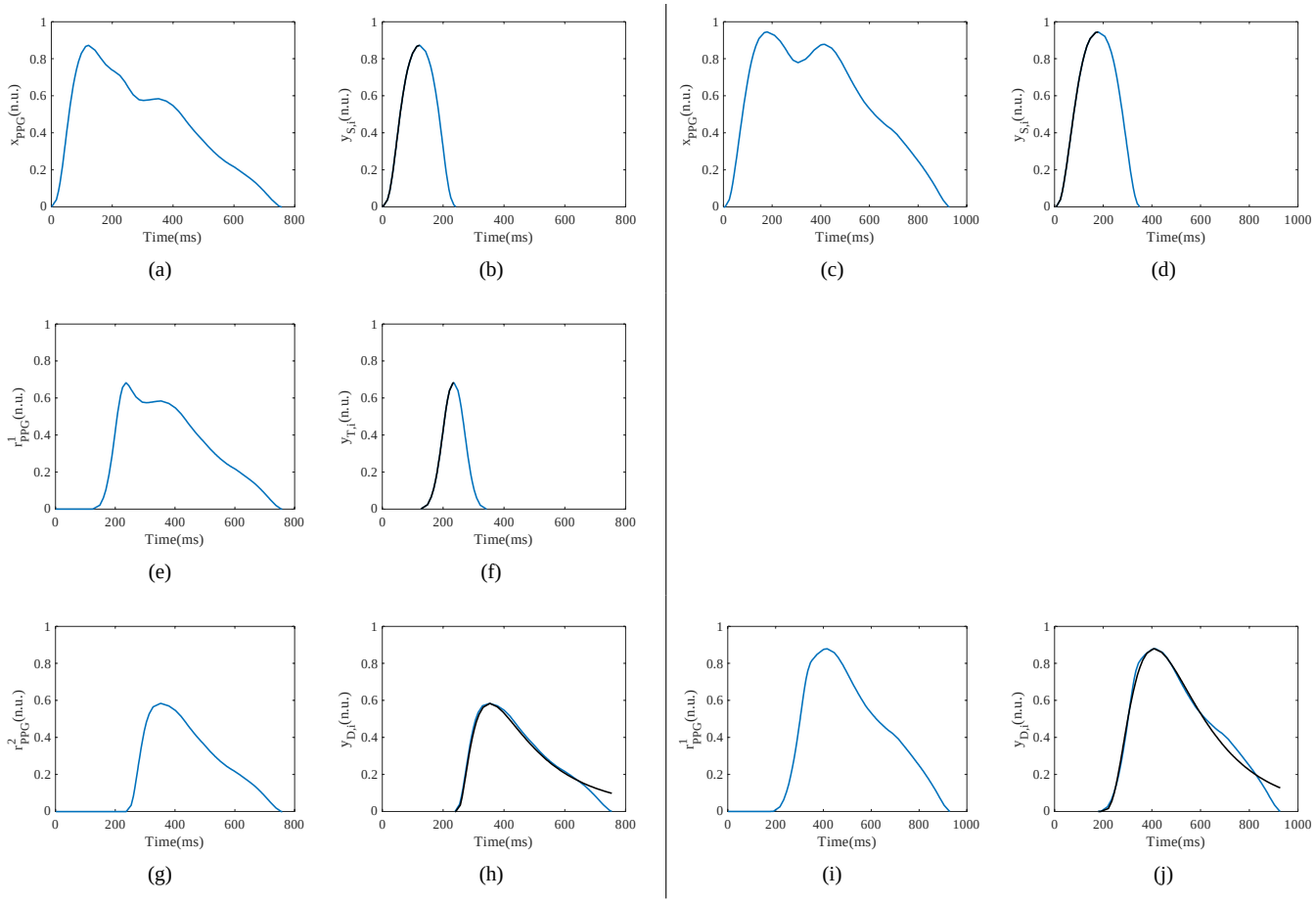

Fig. 2. Example of the entire algorithm, with three waves (left) and with two waves (right). Firstly, a) and c) represents the original PPG pulse ($x_{PPG}(n)$); b) and d) represents the extraction of the wave related to the systolic peak ($y_{S,i}(n)$), with the up-slope (that it is horizontally flipped) highlighted in black. Secondly, e) and i) represents the first residual pulse waveform ($r^1_{PPG}(n)$), obtained as the subtraction of $y_{S,i}(n)$ from $x_{PPG}(n)$; in f) the time duration of the maximum of $r^1_{PPG}(n)$ is shorter than the 35% of the complete pulse time duration, so a new wave ($y_{T,i}(n)$) not related with the diastolic peak is extracted, with the up-slope (that it is horizontally flipped) highlighted in black. Then, g) represents the second residual pulse waveform ($r^2_{PPG}(n)$), obtained as the subtraction of $y_{T,i}(n)$ from $r^1_{PPG}(n)$. Finally, in h) and j) the time duration of the maximum is longer than the 35% of the complete pulse time duration, so both waves are related with the diastolic peak and they are modelled as lognormal waves ($y_{D,i}(n)$, in black).

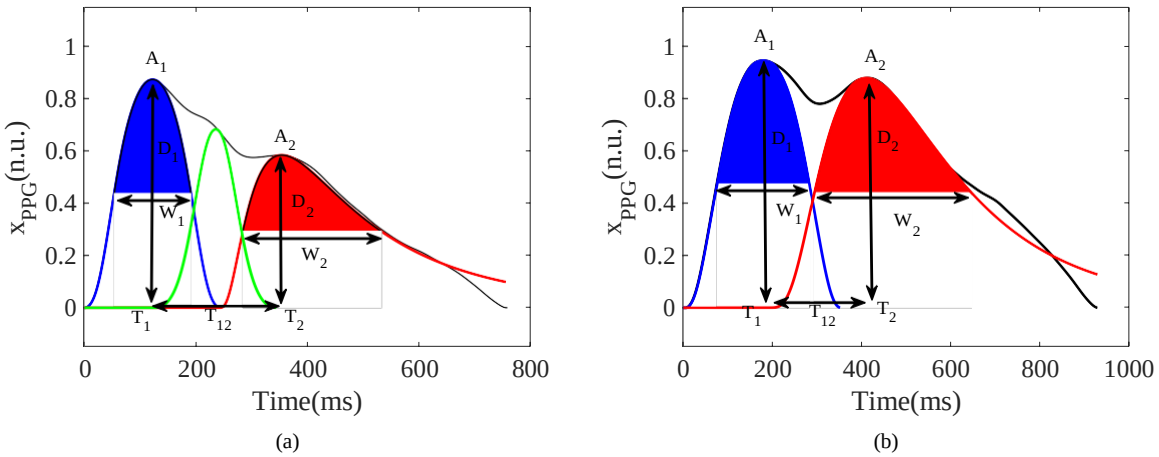

Fig. 3. Example of the amplitude (A1 and A2), position (T1 and T2), width (W1 and W2), area (D1 and D2) and time delay (T12) in two PPG pulses, the first one decomposed with three waves (a) and the second one decomposed with two waves (b).

$$RC(Y_X) = \frac{Y_X - Y_{1D}}{Y_{1D}} \cdot 100, \quad (3)$$

where X can be 3D, 5, 3A or 1A.

The Shapiro-Wilk test was used to check normality of the relative change $RC(Y_X)$. If the normal distribution of one ratio was verified, the t-Student paired test was applied. Otherwise, the Wilcoxon paired test was used. A p-value $< \alpha$ defines significance in value with respect to reference state S1D, where the significance level α can be 0.05, 0.01 or 0.001. This test allows identifying significant differences in each parameter, for each stage with respect to the basal state. Finally, a test using ANOVA statistics (or Friedman for non-parametric distributions) for multiple comparisons was applied. If statistically significant difference between groups exists, then a post-hoc analysis with T-Student (or Wilcoxon) using Bonferroni correction was applied to assess the differences between the estimated *RCs* of the four stages [47].

IV. Results

The final number of subjects were 23 subjects in S1D and S3D, 18 in S5, 19 in S3A and 17 in S1A, since some subjects could not be recorded properly in all the stages due to a poor PPG signal quality.

About the two different pulse decompositions presented in this work, the 33,44% of the total number of pulses are decomposed in two waves and the 66,56% of the total number of pulses are decomposed in three waves. Fig. 4 shows the mean and the standard deviation of all the pulses for two different subjects, one decomposed in three waves and the other in two, in the five stages. The average decomposition in Gaussians and lognormals waves is also represented.

Fig. 5 shows the RC in the amplitude (A1 and A2), the position (T1 and T2), the width (W1 and W2) and the area (D1 and D2) of the first and second waves of the PPG pulse associated with the systolic and the diastolic peaks. The RC of the pulse-to-pulse interval (T_{BB}), the time delay between both waves (T12), the ratio between the width (W2/W1), and the ratio between the areas (D2/D1) are also shown. Results showed two different trends. On the one hand, T_{BB}, T2, T12, W1 and W2 showed significant differences between the initial stages with the final stages, increasing or decreasing their value. In these boxplots, there was a significant difference of S5, S3A and S1A with the first stage of the protocol, S1D (indicated with the asterisks in the lower part of the boxplot). Also, in these parameters (except W1), there was a significant difference of the last 3 stages with the second one (S3D), as the arrows pointed out. On the other hand, T1, A1, A2, W2/W1, D1 and D2/D1 reached its minimum or its maximum in the deepest stage, S5, with significant differences with stage S1D (reflected by asterisks) and the other 3 stages (reflected by arrows).

V. Discussion

In this work, 13 morphological parameters extracted from the PPG pulse wave were analyzed to find differences due to the effect of the pressure in a database recorded inside a hyperbaric chamber. To do that, five different stages with three different pressures (1, 3 and 5 atm) were analyzed and the PPG signal was recorded in each of these stages. Each PPG pulse was isolated and two waves were extracted from them. The first one, related to the systole, was extracted directly from the pulse, by concatenating the up-slope from the beginning to the maximum with itself flipped horizontally. The second wave, related with the diastole, was modelled by a lognormal wave whose maximum matched with the maximum associate with the diastolic peak. From these two waves, the amplitude, the time of their maximum, the width and the area under these curves were calculated, together with some ratios, to find out if there were changes in these parameters due to the pressure or the time spent inside the chamber.

The main novelty of this work is the algorithm to extract two waves related to the systole and the diastole and whose peaks match with the systolic and the diastolic peaks, since with other methods explained in the literature this goal was not reached. The association of decomposed waves to their physiological meaning is complicated due to the existence of different morphologies, so the same decomposed wave could reflect a different physiological phenomenon depending on the PPG morphology. Our first approach was to apply several algorithms found in the literature that models the PPG pulse as a main wave superposed with several reflected waves based on different shapes including Gaussians [32], [33], [34], lognormals [35], Rayleighs [36] or a combination of them [37], [38]. However, the decomposed waves of these models did not match with the systolic and diastolic peaks, or the amplitude of the waves was not enough to extract amplitude parameters. Therefore, this strategy was discarded. The alternative was using a pulse decomposition analysis based on extracting the waves one-by-one, as the one used in previous works [40], [41]. This algorithm obtains three waves using the up-slope of the pulse concatenated with itself horizontally flipped and it models each wave as a Gaussian. In this database, this algorithm fits with the first peak and is able to characterize the systolic peak, however, when the first wave is subtracted and the residual PPG waveform is obtained, the up-slope of this new pulse is usually more abrupt than the down-slope. This caused a problem, since with the use of three waves as in [40], [41] it was impossible to decompose the entire pulse. Therefore, the alternative that we propose in this work is using a lognormal wave to characterize the diastolic part of the PPG pulse, since its down-slope is smoother than its up-slope and this type of curve fits better with the tail of the PPG pulse wave.

In fact, the approximation of modelling each part of the PPG pulse separately is not new in the literature, for example in [39] the anacrotic and catatrotic phases were modelled separately. Once the type of wave to model the diastolic phase was established, it was necessary that the maximum peak of the residual PPG waveform matched with the diastolic peak. It must be noticed that when the wave associated to the systolic part is subtracted from the original PPG pulse, then the new maximum of the residual PPG waveform is usually found at the beginning of the new waveform instead of being in the diastolic peak. If this happens, the same algorithm explained

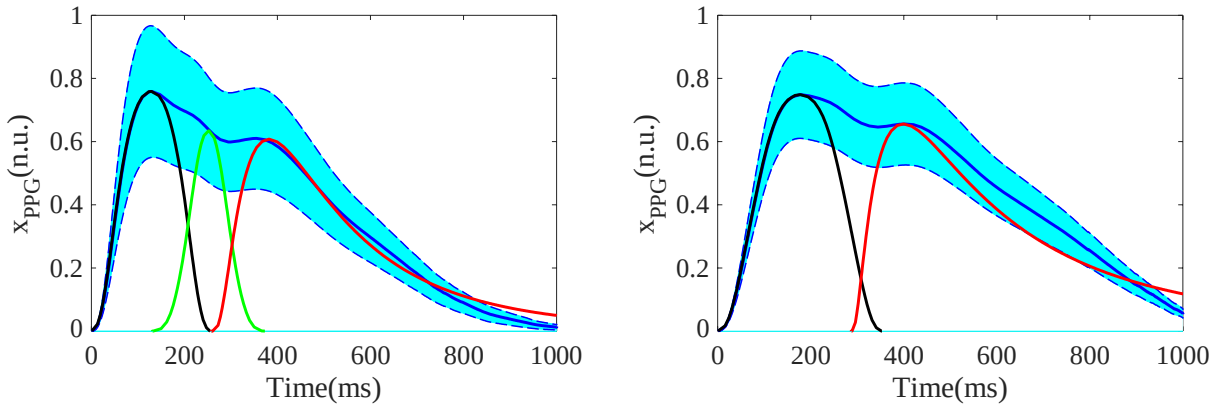

Fig. 4. Average pulse waveforms for two subjects in the five pressure stages. The blue lines and shaded areas represent the ensemble average and standard deviation, respectively. The average decomposition in two or three waves is also represented: in black, the first Gaussian wave related with the systolic part; in green, the second Gaussian wave (if needed); in red, the lognormal wave related with the diastolic part.

for the first wave is repeated one more time in our proposal, obtaining a transition second wave. This wave is only used in the decomposition process to obtain the pulse wave related to diastole and no parameters are extracted for it. Although it could include physiological information it's not considered, as this study is focused only on the systolic and diastolic waves. Again, the new maximum of the residual PPG pulse (with the subtraction of one or two waves if necessary) is located, and this value does match with the diastolic peak, so this part can be modelled as the diastolic part. The way to determine if this maximum belongs to the diastolic peak or not (in other words, if the second wave extracted only for subtraction is needed) is by setting a temporal threshold: if the temporal location of the maximum is higher than the 35% of the pulse wave duration, this peak belongs to the diastolic part; if not, the maximum is located in the transition part and the second wave is obtained and subtracted from the resultant pulse waveform. The 35% threshold was selected because left ventricular ejection time related with the systole usually lasts less than 35% of the pulse wave duration [46]. The establishment of this threshold is the other main novelty in this work. Experimentally, it has been proven that this threshold, in this population, allows us to correctly detect the diastolic peak and it is always reached in two iterations of the proposed algorithm at maximum. However, in other databases with different type of population this threshold could vary. Another possible way to determine if the maximum belongs to the diastolic part could be the maximum after the dicrotic notch. However, this point is not easy to identify in all pulses, so this was the reason to establish a temporal threshold.

Once the rest of the PPG pulse related to the diastolic part is determined, the resultant pulse can be modelled as a lognormal wave, whose amplitude, width, and area characterize the diastolic part of the PPG pulse. Therefore, the resultant pulse is modelled as a lognormal wave, fitting μ and σ to minimize the mean-squared error between the lognormal wave and the resulting pulse waveform. The main problem of this type of wave is that the end part of the down-slope do not return to the zero value, therefore the width and the area under the curve were calculated using the 50% of amplitude instead of the 100%.

Morphological parameters were extracted from the systolic and diastolic waves and the Relative Change (RC) of each parameter (Y_X) with respect to the reference stage (1D) was computed in order to minimize the effects of the inter-subject variability. The parameters associated with the systolic peak (T1, A1, W1 and D1) showed a significant increase in their values when the pressure increased, especially in S5 stage where the maximum pressure was reached. This significant increase is represented in the boxplots with the arrows between S5 and the rest of the stages (S3D, S3A and S1A) and the asterisks below S5 box that marked the significant difference with S1D. The parameters associated with the systolic peak reflect the heart pumping, and they depend on several factors, being the systemic vascular resistance and the arterial compliance two of the most relevant. A possible explanation of the increase in the parameters associated with the systolic peak when the pressure increases could be an increase in the vascular resistance, which is attributable to a vasoconstriction [27]. This effect was explained in a previous work [50], where a vasoconstriction was produced due to an increase in the partial pressure of oxygen when the pressure increases. This vasoconstriction could be related to an activation of the sympathetic system of the subject [21]. Furthermore, a reduction in the arterial diameter could mean that more time is required for the blood to circulate, and therefore it could explain an enlarge in the up-slope of the pulse (W1). In the same way, the ratios computed (RI, W2/W1 and D2/D1) showed a minimum value in the S5 stage, with significant differences with the rest of the stages (as the arrows and asterisks pointed out), except from RI. In [26], they found that the ratio of the two areas, can be used as an indicator of total peripheral resistance. The same conclusion was found in [23], [24] with the ratio of the amplitude of the systolic peak and the diastolic peak of the PPG. Although a physiological interpretation of the ratio between the two widths was not found in the literature, this ratio points out

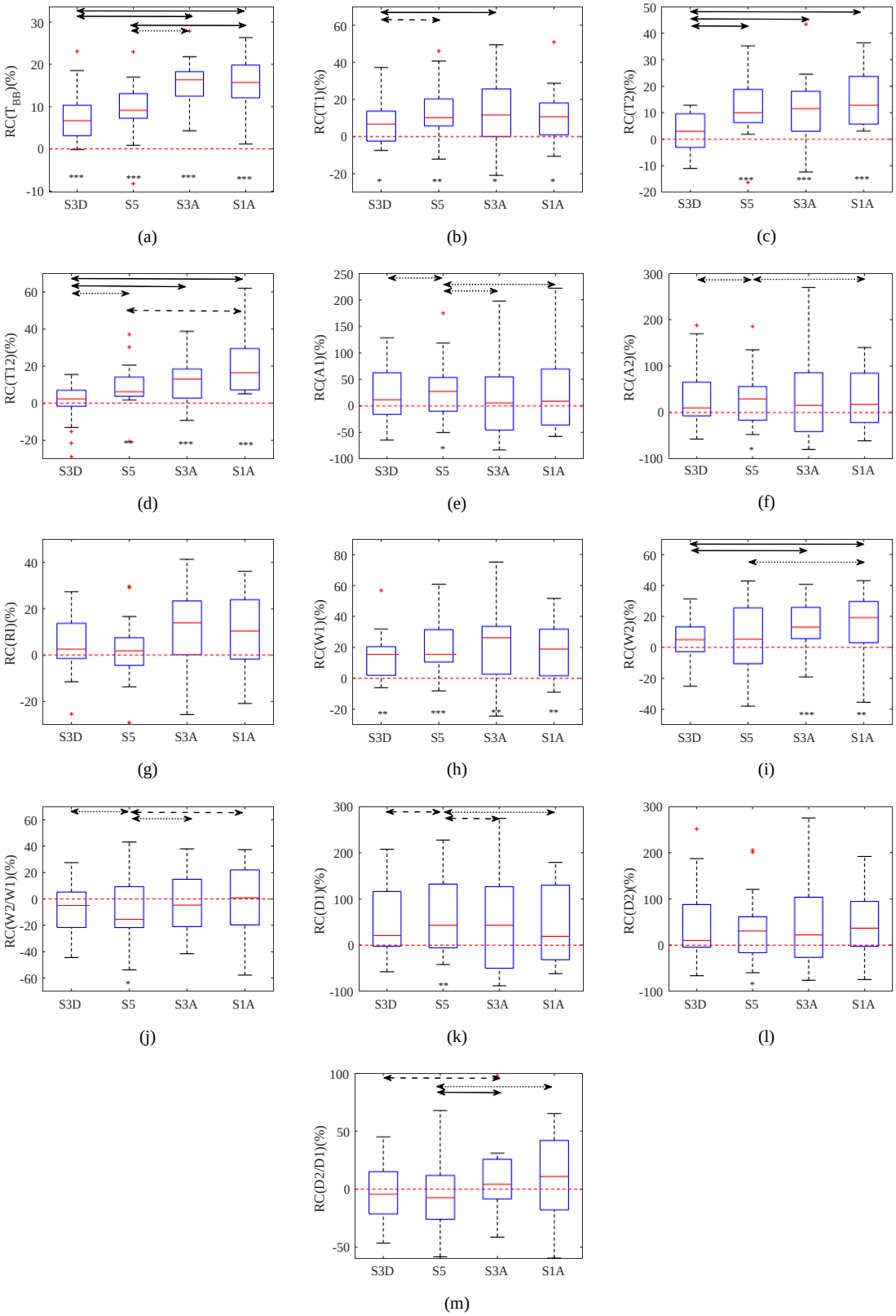

Fig. 5. Boxplots of the RC of the pulse-to-pulse interval (a), the time instant of the first peak, the second peak and the difference among them (b, c and d, respectively), the amplitude of the first peak and the second peak (e and f, respectively), the width of the first and second waves and the ratio between them (g, h and i, respectively) and the area under the curve of the first and second waves and the ratio between them (j, k and l, respectively). Significant differences with the S1D stage are represented by one, two or three asterisks (for α = 0.05, 0.01, and 0.001, respectively). Significant differences between the RC of the four stages are represented by a double arrow (dotted if $p-$value≤0.05, dashed if $p-$value≤0.01 and solid if $p-$value≤0.001).

in the same direction and in the future could also be used as an indicator of total peripheral resistance.

About the parameters related with the diastolic peak (T2, A2, W2 and D2), the value of T2 and W2 increased from the two first stages to the last three ones (as the asterisks for S1D and the arrows for S3D pointed out). Therefore, these two parameters were not only affected by the pressure, but also by the time spent inside the hyperbaric chamber. This dependency with the time could be seen in the pulse- to-pulse interval (T_{BB}), which increased its value during the entire protocol, which implies a decrease in the heart rate. This fact had been reported previously in hyperbaric chamber studies [8], [9], [10], [11], [12] and in immersion data [6], [7]. This dependency with time was also reflected in T12, that increased its value in each stage. The time difference between systolic and diastolic peaks can be used to infer the transit time taken for the PPG wave to propagate along the aorta and large arteries to the major sites of reflection in the lower body and back to the root of the subclavian artery [48], so an increase in T12 could mean a change in PPG pulse contour due to a decrease in large artery stiffness when subjects are inside an hyperbaric environment. When the heart rate decreased (as it did during the protocol), the heartbeat has more time to recover and therefore the down-slope of the pulse is larger (as T12 showed), thus increasing the width of the diastolic part.

As a sum up, with the decomposition of the PPG pulse using this new algorithm it can be shown a dependency with pressure of the parameters of the systolic wave and a dependency with the time spent in the hyperbaric chamber of the parameters of the diastolic wave. On the one hand, the variation in the parameters of the systolic wave could reflect a vasoconstriction related with an increase in pressure, probably due to an activation of the sympathetic system on the blood vessels that increases the systemic vascular resistance [21]. On the other hand, the variation of the parameters associated with the diastolic part depends on the systemic vascular resistance and on an increase in the pulse-to-pulse interval during the entire protocol.

Based on our knowledge, the most similar work to this was the one in [50], where alterations in the morphology of the PPG were studied inside a hyperbaric chamber. One difference among the two studies lies in the separation of the pulses: while in [50] the pulse was divided into the anacrotic and the catatrotic phases, with the maximum of the PPG pulse being the separation of both phases, in this work two waves representing the systolic and diastolic peaks were obtained. In fact, in [50] the difficulty to estimate the location of the dicrotic notch and the diastolic peak was pointed out, so the algorithm presented in this work proposed a robust method to overcome these difficulties and this methodology gives us the opportunity to study some parameters than in the other study were impossible to measure, as the amplitude and the time instant of the peaks, and the time instant difference or the amplitude ratio. Other difference among the studies resides in the way to extract the morphological parameters: while in [50] they were extracted directly from the pulse, in this study they were extracted from the pulse in the first wave and also from the lognormal curve that approximates the diastolic wave. This change in the form to extract the PPG parameters made that they could be computed only at the half maximum in this work, while in [50] they were computed both at the half maximum and at the base. Looking at the results, in [50] the width of the up-slope (similar to W1 here) had a maximum in S3A instead of S5, so the dependency with the pressure was not found with this parameter. Independently of the methodology used, results of both works point out to a vasoconstriction when the pressure increases, probably related with an increased vascular resistance. This vasoconstriction could be produced by the increase in partial pressure of oxygen that occurs inside the hyperbaric environments [51].

Therefore, this new algorithm allows us to decompose PPG pulses in its systolic and diastolic waves, and to extract their parameters without the need to correctly locate the dicrotic notch in the pulse. Results show a dependency of the systolic parameters and the ratios with the pressure and a dependency of the diastolic parameters with the time spent inside the hyperbaric chamber. However, it must be noticed that subjects in this database were young and they have a habit of practicing exercise, therefore more studies with other type of population and other type of analysis instead of the pressure changes must be done to completely validate this new algorithm and to verify the experimental threshold of 35% established in this work. Also, it would be interesting in a future study to analyze the parameters obtained with this decomposition and the ones related with the fiducial points and the first and second derivatives of the PPG [52], [53] to compare the information given by all of them.

VI. Conclusion

In this work, a new methodology to decompose the PPG pulse into two waves was presented. The first wave was related with the systolic part, with its maximum in the systolic peak. The second wave was related to the diastolic part, it was modelled by a lognormal curve, adjusting its maximum to the diastolic peak. This methodology was applied in a hyperbaric chamber database. Results of the parameters related with the systolic part and the ratios pointed out to a vasoconstriction, probably due to an activation of the sympathetic system on the blood vessels, when the pressure increased. Results of the parameters related with the diastolic part reflected the vasoconstriction but also a dependency with the pulse-to-pulse interval. Therefore this methodology offers an alternative to extract parameters related to PPG morphology that are able to distinguish changes in its waveform, at least in hyperbaric environments.

Acknowledgements

This work has been partially financed by Ministerio de Econom´ıa, Industria y Competitividad (MINECO) and by fondos FEDER through the project PGC2018-095936-B-I00 and RTI2018-097723-B-I00; by Centro Universitario de la Defensa (CUD) under the projects CUD2020-11 and UZCUD2020-TEC-03; and by Aragón Government and European Regional Development Fund through Grupos de Referencia BSICoS

(Biomedical Signal Interpretation & Computational Simulation, T39-20R). The authors clarify that this material is the authors' own original work and it reflects the authors' own research and analysis. The results are appropriately placed in the context of prior and existing research. All authors have been involved in substantial work leading to the paper and will take public responsibility for its content. The authors would like to thank Hospital General de la Defensa de Zaragoza, that allowed to use the hyperbaric chamber and the assistance as volunteers of the Regimiento de Pontoneros y Especialidades de Ingenieros n°12.

REFERENCES

[1] E.P. Widmaier, H. Raff, K.T. Strang, "Vander's Human Physiology. The Mechanisms of Body Function", Eleventh ed., McGraw-Hill Higher Education, Boston, 2008.

[2] D.Z. Levett, I.L. Millar, "Bubble trouble: a review of diving physiology and disease", Postgrad. Med. J., 84, 571-578, 2008.

[3] E. Gempp, P. Louge, "Inner ear decompression sickness in scuba divers: a review of 115 cases", Eur. Arch. Otorhinolaryngol., 270, 1831–1837, 2013.

[4] J.D. Schipke, M. Pelzer "Effect of immersion, submersion, and scuba diving on heart rate variability", Br. J. Sports Med., 35, 174-180, 2001.

[5] A.D. Flouris, J.M. Scott, "Heart rate variability responses to a psychologically challenging scuba dive", J. Sports Med. Phys. Fitness, 49(4), 382-386, 2009.

[6] F. Chouchou, V. Pichot, M. Garet, J.C. Barthelemy, F. Roche, "Dominance in cardiac parasympathetic activity during real recreational scuba diving", Eur. J. Appl. Physiol., 106, 345-352, 2009.

[7] Y. Noh, H.F. Posada-Quintero, Y. Bai, J. White, J.P. Florian, P.R Brink, K.H. Chon, "Effect of Shallow and Deep scuba Dives on Heart Rate Variability", Front. Physiol., 9, 110, 2018.

[8] V. Lund, E. Kentala, H. Scheinin, J. Klossner, H. Helenius, K. Sariola-Heinonen, J. Jalonen, "Heart rate variability in healthy volunteers during normobaric and hyperbaric hyperoxia", Acta Physiol. Scand., 167, 29-35, 1999.

[9] V. Lund, E. Kentala, H. Scheinin, J. Klossner, K. Sariola-Heinonen, J. Jalonen, "Hyperbaric oxygen increases parasympathetic activity in professional divers", Acta Physiol. Scand., 170, 39-44, 2000.

[10] V. Lund, J. Laine, T. Laitio, E. Kentala, J. Jalonen, H. Scheinin, "Instantaneous beat-to-beat variability reflects vagal tone during hyperbaric hyperoxia", Undersea Hyperbar. M., 30, 29-36, 2003.

[11] E. Barbosa, J.M. García-Manso, J.M. Martín-González, S. Sarmiento, F.J. Calderón, M.E. Da Silva-Grigoletto, "Effect of Hyperbaric Pressure During scuba Diving on Autonomic Modulation of the Cardiac Response: Application of the Continuous Wavelet Transform to the Analysis of Heart Rate Variability", Mil. Med., 175(1), 61-64, 2010.

[12] A. Hernando, M.D. Peláez-Coca, M.T. Lozano, M. Aiger, D. Izquierdo, A. Sánchez, M.I. López-Jurado, I. Moura, J. Fidalgo, J. Lázaro, E. Gil, "Autonomic nervous system measurement in hyperbaric environments using ECG and PPG signals", IEEE J. Biomed. Health Inform., 23(1), 132-142, 2019.

[13] S. Lu, H. Zhao, K. Ju, K. Shin, M. Lee, K. Shelley, K. Chon, "Can photoplethysmography variability serve as an alternative approach to obtain heart rate variability information?", J. Clin. Monit. Comput., 22, 23-29, 2008.

[14] N. Selvaraj, A.K. Jaryal, J. Santhosh, K.K. Deepak, S. Anand, "Assessment of heart rate variability derived from finger-tip photoplethysmography as compared to electrocardiography", J. Med. Eng. Technol., 32, 479-484, 2008.

[15] K. Charlot, J. Cornolo, J.V. Brugniaux, J.P. Richalet, A. Pichon, "Interchangeability between heart rate and photoplethysmography variabilities during sympathetic stimulations", Physiol. Meas., 30, 1357-1369, 2009.

[16] E. Gil, M. Orini, R. Bailón, J.M. Vergara, L. Mainardi P.Laguna, "Photoplethysmography pulse rate variability as a surrogate measurement of heart rate variability during non-stationary conditions", Physiol. Meas., 31, 1271-1290, 2010.

[17] A.V.J. Challoner, "Photoelectric plethysmography for estimating cutaneous blood flow", Non-Invasive Physiological Measurements(1), 125-51, ed P. Rolfe (London: Academic), 1979.

[18] K.H. Shelley, "Photoplethysmography: beyond the calculation of arterial oxygen saturation and heart rate", Anesth. Analg., 105(6), S31-S36, 2007.

[19] J. Allen, "Photoplethysmography and its application in clinical physiological measurement", Physiol. Meas., 28(3), R1, 2007.

[20] J.C. Dorlas, J.A. Nijboer, "Photo-electric plethysmography as a monitoring device in anaesthesia. Application and interpretation". Br. J. Anaesth., 57, 524-30, 1985.

[21] M. Elgendi, "On the analysis of fingertip photoplethysmogram signals", Curr. Cardiol. Rev., 8(1), 14-25, 2012.

[22] C.C.Y. Poon, X.F. Teng, Y.M. Wong, C. Zhang, Y.T. Zhang, "Changes in the photoplethysmogram waveform after exercise", Med. Devices Sens., 115-118, 2004.

[23] K. Takazawa, N. Tanaka, M. Fujita, O. Matsuoka, T. Saiki, M. Aikawa, S. Tamura, C. Ibukiyama, "Assessment of vasoactive agents and vascular aging by the second derivative of photoplethysmogram waveform", Hypertension, 32(2), 365-370, 1998.

[24] J.M. Padilla, E.J. Berjano, J. Sáiz, L. Fácila, P. Díaz, S. Mercé, "Assessment of relationships between blood pressure, pulse wave velocity and digital volume pulse", Comput. Cardiol., 33, 893-896, 2006.

[25] S.C. Millasseau, R.P. Kelly, J.M. Ritter, P.J. Chowienczyk, "Determination of age-related increases in large artery stiffness by digital pulse contour analysis", Clin. Sci., 103(4), 371-377, 2002.

[26] L. Wang, E. Pickwell-MacPherson, Y.P. Liang, Y.T. Zhang, "Noninvasive cardiac output estimation using a novel photoplethysmogramindex", Annu. Int. Conf. IEEE Eng. Med. Biol. Soc., 1746-1749, 2009.

[27] A.A. Awad, A.S. Haddadin, H. Tantawy, T.M. Badr, R.G. Stout, D.G. Silverman, K.H. Shelley, "The relationship between the photoplethysmographic waveform and systemic vascular resistance", J. Clin. Monit. Comput., 21(6), 365-372, 2007.

[28] M.D. Peláez-Coca, M.T. Lozano, A. Hernando, M. Aiger, E. Gil, "Photoplethysmographic waveform versus heart rate variability to identify low-stress states: Attention test", IEEE J. Biomed. Health Inform., 23(5), 1940-1951, 2019.

[29] Y. Li, H. Yan, Z. Xu, M. Wei, B. Zhang, Z. Shi, "Analysis of the changes in photoplethysmogram induced by exercise stress", J. Med. Imaging Health Inform., 3(3), 347-355, 2013.

[30] A. Wang, L. Yang, C. Liu, J. Cui, Y. Li, X. Yang, S. Zhang, D. Zheng, "Athletic Differences in the Characteristics of the Photoplethysmographic Pulse Shape: Effect of Maximal Oxygen Uptake and Maximal Muscular Voluntary Contraction", Biomed. Res. Int., 8, 2015.

[31] S.P. Linder, S.M. Wendelken, E. Wei, S.P. McGrath, "Using themorphology of photoplethysmogram peaks to detect changes in posture", J. Clin. Monit. Comput., 20(3), 151-158, 2006.

[32] M.C. Baruch, D.E. Warburton, S.S. Bredin, A. Cote, D.W. Gerdt, C.M. Adkins, "Pulse Decomposition Analysis of the digital arterial pulse during hemorrhage simulation", Nonlinear Biomed. Phys., 5(1), 1, 2011.

[33] L. Wang, L. Xu, S. Feng, M.Q.H. Meng, K. Wang, "Multi-Gaussian fitting for pulse waveform using weighted least squares and multi-criteria decision making method", Comput. Biol. Med., 43(11), 1661-1672, 2013.

[34] C. Liu, T. Zhuang, L. Zhao, F. Chang, C. Liu, S. Wei, Q. Li, D. Zheng, "Modelling arterial pressure waveforms using Gaussian functions and two-stage particle swarm optimizer", Biomed. Res. Int., 2014, 923260, 10 pages, 2014.

[35] M. Huotari, A. Vehkaoja, K. Määttä, J. Kostamovaara, "Photoplethysmography and its detailed pulse waveform analysis for arterial stiffness", J. Mech. Mater. Struct., 44, 345-362, 2011.

[36] D. Goswami, K. Chaudhuri, J. Mukherjee, "A new two-pulse synthesis model for digital volume pulse signal analysis", Cardiovasc. Eng., 10, 109-117, 2010.

[37] S.C. Huang, H.Y. Jan, G.H. Lin, W.C. Lin, K.P. Lin, "Decomposition analysis of digital volume pulse signal using multi-model fitting", XIII Mediterranean Conference on Medical and Biological Engineering and Computing 2013, 41, 635-638, 2013.

[38] A. Sološenko, A. Petrėnas, V. Marozas, L. Sörnmo, "Modeling of the photoplethysmogram during atrial fibrillation", Comput. Biol. Med., 81, 130-138, 2017.

[39] U. Rubins, "Finger and ear photoplethysmogram waveform analysis by fitting with Gaussians", Med. Biol. Eng. Comput., 46, 1271-1276, 2008.

[40] J. Lázaro, E. Gil, M. Orini, P. Laguna, R. Bailón, "Baroreflex Sensitivity Measured by Pulse Photoplethysmography", Front. Neurosci., 13:339, 1-13, 2019.

[41] S. Kontaxis, E. Gil, V. Marozas, J. Lázaro, E. García, M. Posadas-de Miguel, S. Siddi, M.L. Bernal, J. Aguiló, J.M. Haro, C. de la Cámara, P. Laguna, R. Bailón, "Photoplethysmographic Waveform Analysis for Autonomic Reactivity Assessment in Depression", IEEE Trans. Biomed. Eng., 68(4), 1273-1281, 2021.

[42] D. Sokas, M. Gailius, V. Marozas, "Diver physiology monitor and its graphical user interface", Virt. Inst. Biomed., 5-9, 2016.

[43] J. Lázaro, E. Gil, R. Bailón, A. Mincholé, P. Laguna, "Deriving respiration from photoplethysmographic pulse width", Med. Biol. Eng. Comput., 51(1), 233-242, 2013.
[44] E. Gil, J.M. Vergara, P. Laguna, "Detection of decreases in the amplitude fluctuation of pulse photoplethysmography signal as indication of obstructive sleep apnea syndrome in children", Biomed. Signal Process. Control., 3(3), 267-277, 2008.
[45] J. Lázaro, E. Gil, J.M. Vergara, P. Laguna, "Pulse rate variability analysis for discrimination of sleep-apnea-related decreases in the amplitude fluctuations of pulse photoplethysmographic signal in children", IEEE J. Biomed. Health Inform., 18(1), 240-246, 2014.
[46] P.H. Charlton, J.M. Harana, S. Vennin, Y. Li, P. Chowienczyk, J. Alastruey, "Modeling arterial pulse waves in healthy aging: a database for in silico evaluation of hemodynamics and pulse wave indexes", Am. J. Physiol. Heart. Circ. Physiol., 317, H1062-H1085, 2019.
[47] R.A. Armstrong, "When to use the Bonferroni correction", Ophthalmic Physiol. Opt., 34, 502-508, 2014.
[48] P.J. Chowienczyk, R.P. Kelly, H. MacCallum, S. Millasseau, T. Andersson, R. Gosling, J. Ritter, E. Anggard, "Photoplethysmographic assessment of pulse wave reflection: blunted endothelium-dependent response to beta$_2$ adrenergic vasodilation in type II diabetes", J. Am. Coll. Cardiol., 34, 2007-2014, 1999.
[49] Y.K. Qawqzeh, M.B.I. Reaz, O. Maskon, K. Chellappan, M.A.M. Ali, "Photoplethysmogram reflection index and aging", Proc. SPIE 8285, International Conference on Graphic and Image Processing (ICGIP 2011), 82852R, 2011.
[50] M.D. Peláez-Coca, A. Hernando, M.T. Lozano, C. Sánchez, D. Izquierdo, E. Gil, "Photoplethysmographic Waveform and Pulse Rate Variability Analysis in Hyperbaric Environments", IEEE J. Biomed. Health Inform., 2021.
[51] C.R. Mortensen, "Hyperbaric oxygen therapy", Curr. Anaesth. Crit. Care, 19(5-6), 333-337, 2008.
[52] S. Sun, R. Bezemer, X. Long, J. Muehlsteff, R.M. Aarts, "Systolic blood pressure estimation using PPG and ECG during physical exercise", Physiol Meas., 37(12), 2154-2169, 2016.
[53] S. Sun, E. Bresch, J. Muehlsteff, L. Schmitt, X. Long, R. Bezemer, I. Paulussen, G.J. Noordergraaf, R.M. Aarts, "Systolic blood pressure estimation using ECG and PPG in patients undergoing surgery", Biomed. Signal Process. Control, 79(1), 104040, 2023.

TBB					
Tipo test	Etapa	S3D	S5	S3A	S1A
T Test	S1D	**8.95*E-7**	**3.42*E-5**	**5.20*E-9**	**7.12*E-8**
ANOVA Test with Bonferroni correction	S3D		0.162	**1.73*E-5**	**8.45*E-4**
	S5			**3*E-4**	**0.033**
	S3A				0.897
	S1A				

A1					
Tipo test	Etapa	S3D	S5	S3A	S1A
T Test	S1D	0.669	**0.048**	0.44	0.788
Friedman Test with Bonferroni correction	S3D		**0.018**	0.059	0.439
	S5			**0.033**	**0.041**
	S3A				0.071
	S1A				

W1					
Tipo test	Etapa	S3D	S5	S3A	S1A
Wilcoxon Test	S1D	**0.002**	**0.001**	**0.004**	**0.004**
Friedman Test with Bonferroni correction	S3D		0.157	0.346	0.796
	S5			0.593	0.989
	S3A				0.439
	S1A				

D1					
Tipo test	Etapa	S3D	S5	S3A	S1A
Wilcoxon Test	S1D	0.223	**0.006**	0.717	0.326
Friedman Test with Bonferroni correction	S3D		**0.018**	0.345	0.796
	S5			**0.033**	**0.044**
	S3A				0.071
	S1A				

T1					
Tipo test	Etapa	S3D	S5	S3A	S1A
Wilcoxon Test	S1D	**0.023**	**0.003**	**0.013**	**0.012**
Friedman Test with Bonferroni correction	S3D		**0.005**	**0.006**	0.071
	S5			0.782	0.564
	S3A				0.197
	S1A				

A2					
Tipo test	Etapa	S3D	S5	S3A	S1A
T Test	S1D	0.465	**0.043**	0.865	0.455
Friedman Test with Bonferroni correction	S3D		**0.018**	0.346	0.439
	S5			0.109	**0.045**
	S3A				0.071
	S1A				

W2					
Tipo test	Etapa	S3D	S5	S3A	S1A
T Test	S1D	0.335	0.365	**0.001**	**0.002**
ANOVA Test with Bonferroni correction	S3D		0.578	**0.006**	**0.004**
	S5			0.141	**0.036**
	S3A				0.125
	S1A				

D2					
Tipo test	Etapa	S3D	S5	S3A	S1A
T Test	S1D	0.307	**0.04**	0.445	0.171
Friedman Test with Bonferroni correction	S3D		0.157	0.637	0.439
	S5			0.285	0.96
	S3A				0.071
	S1A				

T2					
Tipo test	Etapa	S3D	S5	S3A	S1A
T Test	S1D	0.141	**0.001**	**0.001**	**0.001**
Friedman Test with Bonferroni correction	S3D		**8.54*E-4**	**0.002**	**0.001**
	S5			0.98	0.96
	S3A				**0.021**
	S1A				

RI					
Tipo test	Etapa	S3D	S5	S3A	S1A
T Test	S1D	0.22	0.739	0.106	0.098
ANOVA Test with Bonferroni correction	S3D		0.45	0.072	0.489
	S5			0.066	0.979
	S3A				0.719
	S1A				

W2/W1					
Tipo test	Etapa	S3D	S5	S3A	S1A
T Test	S1D	0.078	**0.043**	0.541	0.558
ANOVA Test with Bonferroni correction	S3D		**0.039**	0.075	0.229
	S5			**0.008**	**0.05**
	S3A				0.669
	S1A				

D2/D1					
Tipo test	Etapa	S3D	S5	S3A	S1A
T Test	S1D	0.391	0.168	0.488	0.946
Friedman Test with Bonferroni correction	S3D		0.637	**0.018**	0.071
	S5			**0.001**	**0.021**
	S3A				0.796
	S1A				

T12					
Tipo test	Etapa	S3D	S5	S3A	S1A
T Test	S1D	0.897	**0.007**	**6*E-4**	**0.001**
Friedman Test with Bonferroni correction	S3D		**0.008**	**0.004**	**0.001**
	S5			0.98	**0.004**
	S3A				0.054
	S1A				